ChemPlusChem

Research Article
doi.org/10.1002/cplu.202500014

Chemistry Europe
European Chemical Societies Publishing

www.chempluschem.org

VIP *Very Important Paper*

Shape-Persistent Anthracene-Based Macrocycles Prepared by Reversible Boronic Ester Formation: Crystallization and Structural Analysis

Shoma Kasahara,[a] Hironobu Hayashi,*[b] Takayuki Okumura,[c] Michio Matsumoto,[d] Mitsuaki Yamauchi,[a] Yoshiyuki Mizuhata,[a] Naoki Aratani,[c] and Hiroko Yamada*[a]

Shape-persistent macrocycles with confined inner spaces have gained significant interest due to their unique properties and potential applications in gas/molecular recognition, nanoscale templates, and nanoelectronics. In this study, we present an efficient synthesis of macrocycles containing anthracene units through reversible boronic ester formation between 1,2-diols and boronic acids. These template-free macrocycles exhibited diverse internal cavities ranging from 11 Å to 20 Å and readily crystallized in solution and on solid substrates. Powder X-ray diffraction analysis revealed that the crystallinity remained after solvent removal. Single crystal X-ray analysis provided detailed insights into the molecular geometry and packing structure. Notably, a macrocycle with phenyl linkers resembles a pseudo-nanocapsule, as the bulky substituents on both sides of the macrocycles prevented the cavity filling by neighbouring molecules. Consequently, the crystalline powders of the macrocycle with phenyl linkers maintained its crystallinity even after annealing, likely resulting in the highest N_2 gas adsorption properties among synthesized macrocycles. This work highlights a robust synthesis strategy for macrocycles, broadening their potential for advanced applications and enabling self-assembled nanoarchitectures.

Introduction

Macrocycles with confined inner space have gained significant attention because they often exhibit specific property depending on the structure and size of cavity.[1–7] Specifically, shape persistent macrocycles have been regarded as important materials for gas/molecular recognition, which contributes to separate or storage desired materials from a mixture of products.[1,3–16] Additionally, accumulating crystalline or self-assembled macrocycles on a substrate in an orderly manner through solution process, they can be utilized as nanoscale templates or patterning materials, and can also be used in the fabrication of nanoelectronics devices and the design of circuits at the nanometer scale.[17–21] These properties and applications are influenced by the size and shape of the cavities as well as the electronic feature of organic moieties. Therefore, to enhance and diversify these properties, it is essential to develop efficient methods for synthesizing macrocycles with various shapes and cavity size with crystalline nature. In spite of these attractive features of macrocycles, the reaction yields of macrocyclization are often low, because of the competing undesirable polymerization.[22,23]

The utilization of dynamic covalent bond offers a promising way for the selective formation of desired structure by controlling the reaction equilibrium.[24–35] Specifically, boronic esters can be readily synthesized by mixing boronic acids with alcohols such as 1,2- and 1,3-diol.[9,34,35] This reversible reaction has been employed to construct not only macrocycles but also complex structures such as molecular organic cages,[36–41] covalent organic frameworks (COFs), and two-dimensional porous nanosheets.[42]

Herein, we present the efficient synthesis of a set of shape-persistent macrocycles containing anthracene units, utilizing reversible boronic ester formation between 1,2-diols and boronic acids. Anthracene derivatives, which possess rigid and planar structures with high air stability, show reasonable solubility together with easy chemical modification to tune the packing structure.[43–45] Additionally, anthracene and its derivatives were utilized as building blocks for the construction of macrocyclic arenes.[46,47] The macrocycles were synthesized without the use of any template molecules, with a variety of internal cavities depending on organic linker molecules. These macrocycles readily crystallized in liquid phase and on substrates. The crystallinity was maintained after solvent removal. Finally, we

[a] *S. Kasahara, Dr. M. Yamauchi, Prof. Dr. Y. Mizuhata, Prof. Dr. H. Yamada*
Institute for Chemical Research
Kyoto University
Gokasho, Uji, Kyoto 611-0011, Japan
E-mail: hyamada@scl.kyoto-u.ac.jp

[b] *Dr. H. Hayashi*
Center for Basic Research on Materials
National Institute for Materials Science (NIMS)
1-2-1 Sengen, Tsukuba, Ibaraki 305-0047, Japan
E-mail: HAYASHI.Hironobu@nims.go.jp

[c] *T. Okumura, Prof. Dr. N. Aratani*
Division of Materials Science
Nara Institute of Science and Technology (NAIST)
8916-5 Takayama-cho, Ikoma, Nara 630-0192, Japan

[d] *Dr. M. Matsumoto*
International Center for Nanoarchitectonics (MANA)
National Institute for Materials Science (NIMS)
1-1 Namiki, Tsukuba, Ibaraki 305-0044, Japan

Supporting information for this article is available on the WWW under https://doi.org/10.1002/cplu.202500014

investigated the surface areas of obtained crystalline powders based on the gas adsorption.

Results and Discussion

The general synthetic scheme for macrocycles was shown in Figure 1. Firstly, an anthracene derivative, **Ant-OH**, with two sets of fixed *cis*-1,2-diol units positioned on the same face of a nearly planar anthracene framework was specifically designed. The orientation of these two sets of fixed *cis*-1,2-diol units is reasonable for the macrocyclization with diboronic acid derivatives.[9,34,35] Triisopropylsiliy(TIPS)ethynyl groups were introduced at the 9,10-positions of anthracene. The presence of TIPSethynyl groups on both sides of the macrocycles ensures solubility and influences tuning the packing structure of the crystals.[48]

The isomeric mixture of *cis*-1,2-diol was synthesized, following Scheme S1.[49] To achieve macrocyclization, it was necessary to separate **Ant-OH** with bis(*cis*-1,2-diol) from its isomeric mixture. Due to the similar polarity, separating the isomers *via* silica gel column chromatography was challenging. However, it was discovered that the differences in the solubility in chloroform enabled the successful isolation of bis(*cis*-1,2-diol) from the mixture by simply washing with chloroform. Attempts to crystallize the separated **Ant-OH** yielded only plate-like crystals, which were unsuitable for single-crystal X-ray analysis. As a result, **Ant-OH** was further reacted with phenyl boronic acid to produce **Ant-Ph** (Figure 2). Needle-shaped crystals of **Ant-Ph** were successfully obtained through slow diffusion in chloroform with 2-propanol vapor. Single crystal X-ray analysis confirmed the formation of boronic esters, demonstrating that the bis(*cis*-1,2-diol) group of **Ant-OH** reacted with phenyl boronic acid in the desired orientation.[50] Consequently, this structure of **Ant-Ph** proved the successful isolation of the desired **Ant-OH** (*vice versa*).

The macrocyclization of **Ant-OH** with various of diboronic acid derivatives was investigated (Figure 3, Scheme S1). For instance, **Ant-OH** and slight excess molar amount of 4,4'-biphenyldiboronic acid were mixed in methanol at room temperature. This mixture led to the formation of precipitates immediately, which were insoluble in methanol. Indeed, matrix-assisted-laser-desorption/ionization time-of-flight mass spectrometry (MALDI-TOF MS) analysis indicated that macrocycles were rapidly formed within 10 min (Figure S1). After collecting the precipitates by filtration, the ^{1}H NMR spectrum of this crude material suggested that the obtained precipitates contained **BiPh[2+2]** as the main product. However, linear polymetric boronic esters composed of **Ant-OH** and 4,4'-biphenyldiboronic acid, which exhibited broad ^{1}H NMR peaks, needed to be removed (Figure S6). Interestingly, the formation of large macrocycles such as **BiPh[3+3]** were also observed in MALDI-TOF MS spectra of crude solution, although the intensity of these peaks was quite weak. In fact, **BiPh[3+3]** was a minor species regardless of trying the macrocyclization with templates or different solvents,[35,51] as confirmed by the separation with gel permeation chromatography (GPC) (*vide infra*), and it could not be isolated. These results suggest that [2+2] macrocycles appear to be thermodynamically stable, justified by the fact that forming a [3+3] cyclic structure leads to a significantly large dihedral angle in the 1,2-diol groups introduced at the termini of anthracene, making such a cyclic structure unfavorable. Furthermore, the synthesis of [3+3] cyclic structures with similar precursors containing 1,2-diol groups can be selectively achieved using specific molecules/solvents as templates.[35] Finally, the crude material containing **BiPh[3+3]** and undesirable polymers was purified by GPC, giving pure **BiPh[2+2]** in 77% yield. Similarly, the combination of **Ant-OH** with various diboronic acids successfully provided a series of macrocycles such as **Ph[2+2]** (43% yield), **TerPh[2+2]** (83% yield), **Py[2+2]** (87% yield), and **TT[2+2]** (75% yield) (Figure 3).

This macrocyclization reaction requires a protic solvent, specifically methanol. It was reported that transesterification takes place through a borate intermediate formed by the coordination between methanol and the boron atom of the

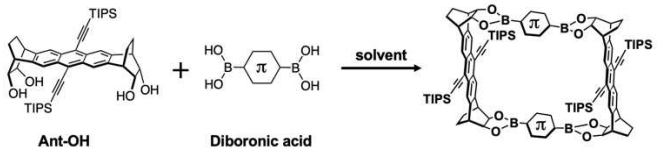

Figure 1. General synthesis for macrocycle employed in this study.

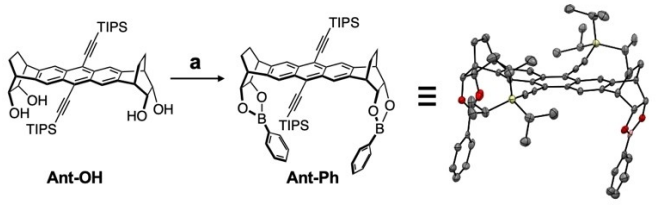

Figure 2. Synthesis of **Ant-Ph** and single crystal X-ray structure of **Ant-OH**. The thermal ellipsoids are shown at 50% probability. Hydrogen atoms and solvent molecules were removed for the clarity. Reaction condition: a) Phenylboronic acid, MeOH, room temperature, 88%.

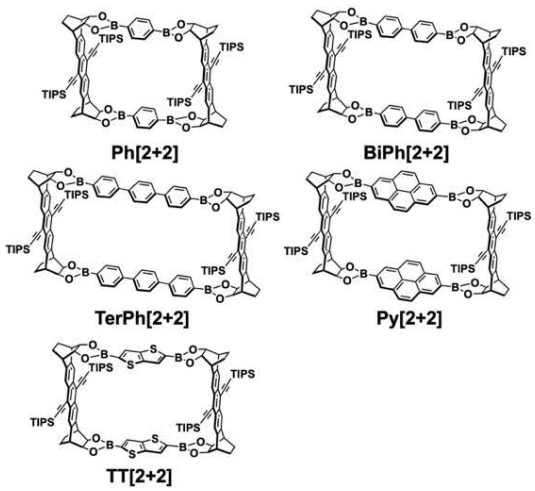

Figure 3. A set of macrocycles synthesized in this study.

molecule.[51] To confirm the formation of macrocycles *via* reversible transesterifications with reasonable yields, the exchange reaction was attempted. Briefly, **BiPh[2+2]** and ten equivalent amounts of pyrene-2,7-diboronic acid were mixed in a mixture of methanol/chloroform (9:1), and stirred for several hours at room temperature. The MALDI-TOF MS spectrum of the reaction mixture clearly showed the formation of **Py[2+2]**, resulting from the dissociation and subsequent re-bonding of the boronic ester units of dissociated species of **BiPh[2+2]** with the 1,2-diol groups of pyrene-2,7-diboronic acid (Figure 4). The observation of macrocycle [1+2+1], comprising pyrene and biphenyl groups, provides additional evidence for the reversible transesterifications. Here, the intensity of MALDI-TOF MS spectrum does not accurately reflect the quantities of products in the system. Note that the formation of precipitates facilitated the isolation of the macrocycle from the system. It is noteworthy that the intermediates of the macrocycle and short linear oligomers exhibit better solubility in methanol than the macrocycle due to the terminal OH groups, which also promotes the transesterification.

Next, the stability of these macrocycles was investigated. Although dynamic covalent bonding is essential for the formation of these macrocycles, ^{1}H NMR measurements and MALDI-TOF-MS revealed that all macrocycles are quite stable once formed in solution. For example, the ^{1}H NMR spectra of **BiPh[2+2]** in $CDCl_3$ showed no significant changes after 48 hours, indicating that the stability of **BiPh[2+2]** (Figure S11). However, the macrocycles gradually decomposed in the presence of bases such as triethylamine, as amine molecules bind to boronic esters.[9] Additionally, the stability in the solid state was also examined. Thermogravimetric analysis (TGA) revealed that all prepared macrocycles showed no significant weight loss below 300 °C, suggesting good thermal stability (Figure S12).

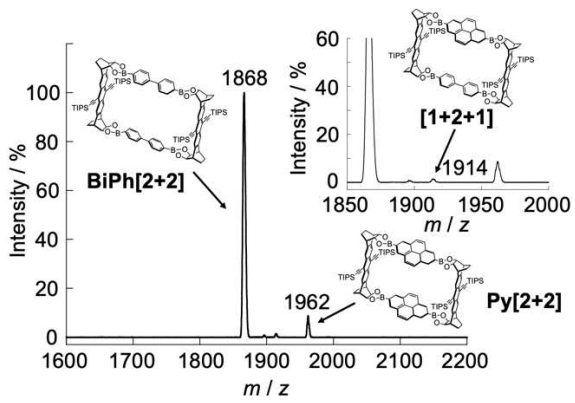

Figure 4. MALDI-TOF-MS spectrum for exchange reactions. Insets shows the magnified region of MALDI-TOF-MS spectrum.

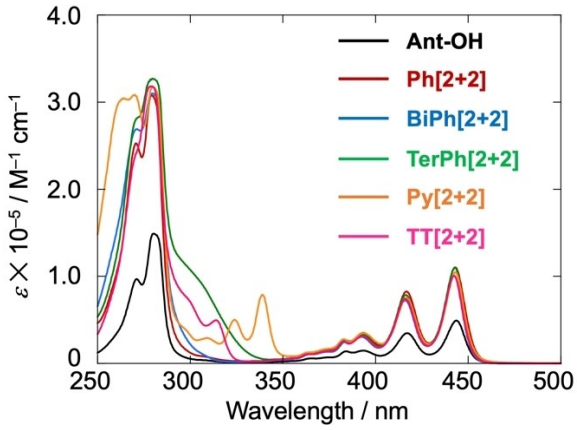

Figure 5. UV-vis absorption spectra of macrocycles in THF.

The optical properties of the macrocycles were examined. UV-vis absorption spectra of the macrocycles in THF are shown in Figure 5. The well-resolved absorption bands of anthracene were clearly observed for macrocycles at 390, 417, and 442 nm, closely matching those of **Ant-OH**, and therefore the macrocyclization gave no effect on the electronic states of anthracenes and organic linker molecules. In addition, the molar extinction coefficients (ε) of the macrocycles were approximately twice the values. These results indicate that there is no specific interaction between the anthracene and the linker units in the ground state. A similar trend was observed in the fluorescence spectra in solution (Figure S13). These macrocycles reflect the good fluorescence feature of **Ant-OH**, with the fluorescence maxima at 511 nm and quantum yields (Φ_f) ranging from 0.82 to 0.84 (Table S1). The fluorescence lifetime was comparable to that of **Ant-OH** (5.4–5.5 ns) (Figure S14).

To gain insight into the molecular geometry in the solid state, single-crystal X-ray analysis was performed (Figure 6). These macrocycles were readily crystallized, although the crystallization required different solvent systems. In all cases, the inner spaces of macrocycles were filled with solvent molecules, while some solvent molecules also occupied the outer spaces of the macrocycles. For instance, in the case of **Ph[2+2]**, the crystal was obtained through the slow evaporation of methanol into an *o*-dichlorobenzene solution of **Ph[2+2]**. Two *o*-dichlorobenzene molecules were packed in the inner space of **Ph[2+2]** (Figure S15). Interestingly, the anthracene backbone was slightly bended (Figure 6a), likely because the boronic ester units of **Ph[2+2]** needed to be flat against the phenyl units in the linker part, causing the anthracene to release strain by bending. In the packing structure, the 5-membered rings containing boronic ester interacted with those in the neighboring macrocycle (closest C•••B distance of 3.4 Å). Additionally, the C_2H_4 bridge of bicyclo[2.2.2]octane moieties, tethered on both sides of the anthracene unit, interacted with anthracene units of the neighboring **Ph[2+2]** through CH–π interactions. These CH–π interactions gave the two-dimensional nanosheet of **Ph[2+2]**. **BiPh[2+2]** and **TerPh[2+2]** also interacted in a similar manner to **Ph[2+2]**. The relatively large inner spaces of **BiPh[2+2]** and **TerPh[2+2]** accommodated the TIPS units to pack **BiPh[2+2]** or **TerPh[2+2]**, forming the one-dimensional alignment of macrocycles. In the case of **TerPh[2+2]**, the anthracene backbone was almost flat, probably because the central phenyl units of terphenyl linker released the strain on the macrocycles, while the linker of **BiPh[2+2]** remained bend. Crystals of **TT[2+2]** suitable for single crystal X-ray analysis were not obtained. Although the quality of crystals for **Py[2+2]** was also not suitable for single crystal X-ray analysis, the preliminary structure and packing could be discussed (Fig-

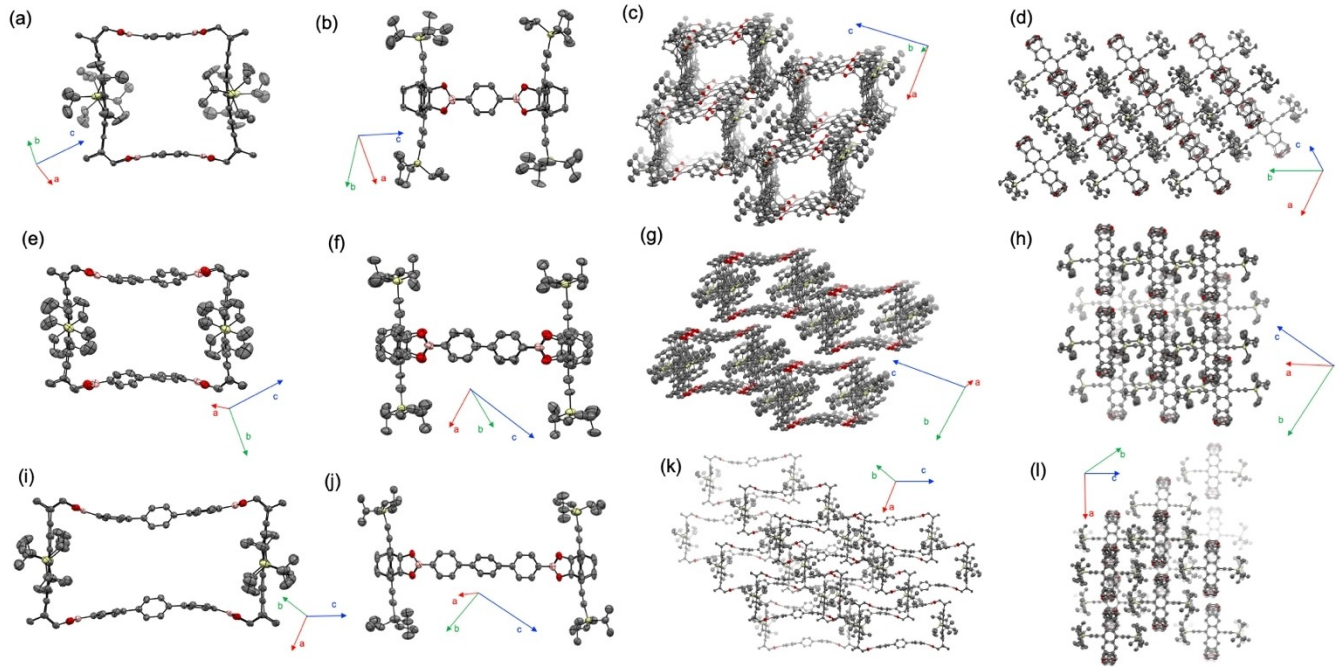

Figure 6. Single crystal X-ray structures of (a,b) **Ph[2+2]**, (e,f) **BiPh[2+2]**, and (i,j) **TerPh[2+2]**. Packing structure of (c,d) **Ph[2+2]**, (g,h) **BiPh[2+2]**, and (k,l) **TerPh[2+2]**. The thermal ellipsoids are shown at 50% probability. Solvent molecules and hydrogen atoms are omitted for clarity.

ure S16). The size of the inner space is almost the same as that of **BiPh[2+2]** due to the same length of pyrene-2,7-diboronic acid and 4,4'-biphenyldiboronic acid. Overall, by changing the linker units, the "width" of macrocycles varied from 11 Å to 20 Å, indicating that these macrocycles can potentially uptake different molecules, depending on the tunable inner size.

The solubility of macrocycles appears to be primarily determined by the size of the inner voids and the presence of bulky TIPS units on both sides of the macrocycles. In fact, the solubilities of **Ph[2+2]**, **BiPh[2+2]**, and **TerPh[2+2]** in chloroform are as follow: 0.12 mg/ml for **Ph[2+2]**, 0.17 mg/ml for **BiPh[2+2]**, and 0.40 mg/ml for **TerPh[2+2]**. Space-filling models for these macrocycles visualized the spaces where solvent molecules might penetrate (Figure S17), supporting that solvent molecules find it difficult to reach the inner space easily, thereby decreasing the solubility, especially in the case of **Ph[2+2]**. Thus, because of the bulky TIPS groups on both sides of the macrocycles, **Ph[2+2]** can be classified as resembling a pseudo-nanocapsule.

The activated crystals of macrocycles were prepared by recrystallization and filtration, followed by drying under vacuum at 100 °C for 3 h. Powder X-ray diffraction (PXRD) analysis revealed that macrocycles maintained their crystallinity after solvent removal (Figure S18). According to the single-crystal X-ray structure analysis, before activating of the macrocycles by heating, the inner cavities of **BiPh[2+2]** and **TerPh[2+2]** were occupied not only by solvent molecules but also by TIPS groups of the neighboring macrocycles, which were positioned to fill the voids within the cavities. Upon filtration and annealing, the solvent molecules in the cavities were removed. This increased the freedom of the TIPS groups of macrocycles, leading to a rearrangement of the packing structure and reducing the usable inner cavities. In fact, prolonged annealing or annealing at 120 °C resulted in broadened PXRD patterns for the crystalline powders of **BiPh[2+2]** and **TerPh[2+2]** (Figure S18), suggesting diminished crystallinities. Conversely, the space-filling model of **Ph[2+2]** clearly shows that TIPS groups of neighboring **Ph[2+2]** macrocycles are unable to fill the inner cavities of a **Ph[2+2]**, because of its short linkers (i.e. phenyl linkers) and bulky TIPS groups. Consequently, in the case of **Ph[2+2]**, the removal of solvent molecules mainly occurs upon the filtration and annealing, preserving its crystallinity. This prevents significant change upon solvent removal and annealing, as evidenced by sharp PXRD pattern observed even after annealing at 140 °C —a stark contrast to **BiPh[2+2]** and **TerPh[2+2]** (Figure S18), highlighting its pseudo-nanocapsule-like nature. Interestingly, the macrocycles readily crystallized on a Si/SiO_2 surface or a glass substrate simply by drop-casting the solution of macrocycles (Figure 7). The changing of interfacial color in the polarized optical microscope

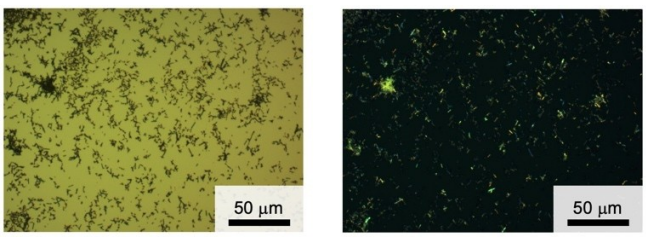

Figure 7. Typical POM images of crystals of **BiPh[2+2]** on a Si/SiO_2 surface. Concentrations for drop-casting of THF solution: 50 μM.

(POM) images indicated the crystallinity of formed needle-like structure.

The crystallinity of macrocycles encouraged us to evaluate their potential application as gas adsorbents. The macrocycles (**Ph[2+2]**, **BiPh[2+2]**, and **TerPh[2+2]**) were crystallized and then filtered followed by drying at 100 °C for 12 hours under vacuum. Then, N_2 sorption isotherms for obtained crystalline powders of macrocycles were measured up to 1 atm at 78 K (Figure 8). Note that our system lacks precision at low relative pressures ($P/P_0 <$ ~0.1). Because of this uncertainty, we assumed that the Brunauer–Emmett–Teller (BET) model could be applied to the N_2 gas adsorption isotherm of **Ph[2+2]** for P/P_0 ranging from 0.155 to 0.245. This approach yielded an apparent surface area of BET = 108 m^2/g (Figure 8, S19). Although this value is modest compared to typical porous materials such as COFs,[42,52] it falls within the range of other arene-based crystalline macrocycles,[53] even though some of which were nonporous (0.9–5.0 m^2/g).[54–57] Interestingly, the BET surface area of macrocycles likely increased as the size of inner cavity decreased. The BET surface areas of **Ph[2+2]**, **BiPh[2+2]**, and **TerPh[2+2]** are as follow: 108 m^2/g for **Ph[2+2]**, 45 m^2/g for **BiPh[2+2]**, and 35 m^2/g for **TerPh[2+2]**. Notably, **Ph[2+2]** clearly exhibited the highest value among these macrocycles. It was initially expected that as the size of the inner cavities of the macrocycles increased, the number of adsorption sites would also increase, thereby leading to a larger BET surface are. However, the results indicated the opposite trend. Based on the single-crystal X-ray structures and PXRD analyses, the following reasons can be considered. As the linkers of the macrocycles become longer, the macrocycles exhibit increased flexibility. For **Ph[2+2]**, the pseudo-nanocapsule-like structure prevents loss of adsorption sites upon solvent removal, whereas **BiPh[2+2]** and **TerPh[2+2]** undergo packing structure rearrangements, reducing available cavities. Consequently, these factors account for **Ph[2+2]** exhibiting larger BET surface area compared to **BiPh[2+2]** and **TerPh[2+2]**.

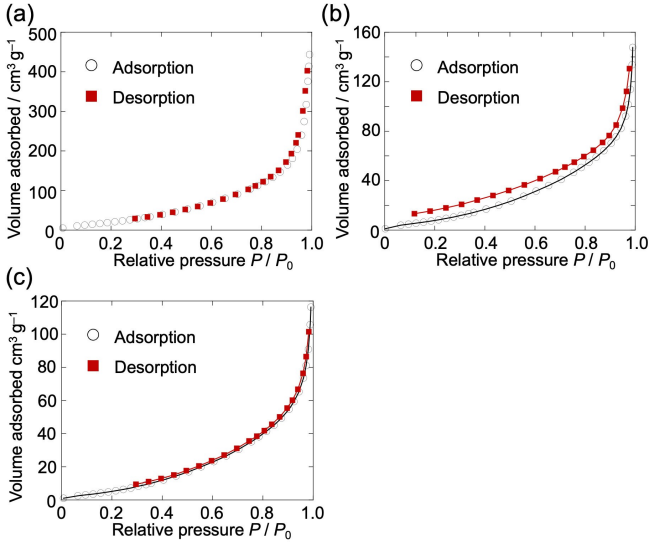

Figure 8. N_2 gas adsorption-desorption isotherm of (a) **Ph[2+2]**, (b) **BiPh[2+2]**, and (c) **TerPh[2+2]**.

Conclusions

In summary, we have successfully synthesized a series of shape-persistent macrocycles containing anthracene units through dynamic covalent bond formation between 1,2-diols and boronic acids. These macrocycles, synthesized without the use of template molecules, feature various internal cavity sizes ranging from 11 Å to 20 Å, and crystallized readily both in solution and on solid substrates. The crystalline nature of the macrocycles was maintained even after solvent removal. Single-crystal X-ray analysis provided insights into the molecular geometry and packing structures. For example, the C_2H_4 bridge of bicyclo[2.2.2]octane moieties in **Ph[2+2]** interacted with anthracene units of the neighboring macrocycles through CH–π interactions. Additionally, **Ph[2+2]** resembles a pseudo-nanocapsule because of its short linkers and the presence of bulky TIPS groups on both sides of the macrocycles. This configuration prevents significant changes of the packing structure upon solvent removal and annealing, which is in stark contrast to **BiPh[2+2]** and **TerPh[2+2]**, where the packing rearrangement occur, reducing usable inner cavities. These findings indicate the crucial role of TIPS groups and linker lengths in determining the usable cavity space, likely accounting for **Ph[2+2]** possessing better N_2 sorption property compared to **BiPh[2+2]** and **TerPh[2+2]**.

Overall, this work demonstrates an efficient synthesis strategy for synthesizing stable and tunable macrocycles. Notably, the TIPS groups on both sides of the macrocycles offer a significant advantage: desilylation followed by coupling reactions such as Sonogashira reactions can introduce various functional groups. This approach not only enables the creation of valuable macrocycles with diverse functional groups but also opens the possibility for constructing organized self-assembled nanoarchitectures, foldamers, molecular machines, and artificial ion channels.[9,58–62]

Supporting Information

The authors have cited an additional reference within the Supporting Information (Ref. [63]). The Supporting Information includes full details of synthesis, additional spectra, details of data collections. Deposition Numbers 2412652 (for **Ant-Ph**), 2412655 (for **Ph[2+2]**), 2412656 (for **BiPh[2+2]**), and 2412657 (for **TerPh[2+2]**) contain the supplementary crystallographic data for this paper. These data are provided free of charge by the joint Cambridge Crystallographic Data Centre and Fachinformationszentrum Karlsruhe Access Structures service.

Acknowledgements

This work was partly supported by JST PRESTO grant No. JPMJPR21AC (HH), JSPS KAKENHI grant Nos. JP20H02816 (HH), JP24K01576 (HH), JP23K26480 (NA), and JP20H05833 (HY), ARIM of MEXT (JPMXP1224NM5302 and JPMXP1224NR5025), JST, the establishment of university fellowships towards the creation of

science technology innovation, grant No. JPMJFS2123 (SK), and JST SPRING, grant No. JPMJSP2110 (SK). We thank Shohei Katao (NAIST) for X-ray crystallographic analysis, Dr. Atsuro Takai (NIMS) for TGA, and Chie Negoro (NIMS) for compound purification.

Conflict of Interests

The authors declare no conflict of interest.

Data Availability Statement

The data that support the findings of this study are available from the corresponding author upon reasonable request.

Keywords: macrocycle · reversible bond formation · crystal · porous material · anthracene

[1] Y. Wang, H. Wu, J. F. Stoddart, *Acc. Chem. Res.* **2021**, *54*, 2027–2039.
[2] M. Iyoda, J. Yamakawa, M. J. Rahman, *Angew. Chem. Int. Ed.* **2011**, *50*, 10522–10553.
[3] D. Talukdar, J. M. Kumar, B. Gole, *Cryst. Growth Des.* **2023**, *23*, 7582–7611.
[4] T. Ogoshi, T. A. Yamagishi, Y. Nakamoto, *Chem. Rev.* **2016**, *116*, 7937–8002.
[5] G. W. Gokel, W. M. Leevy, M. E. Weber, *Chem. Rev.* **2004**, *104*, 2723–2750.
[6] I. Roy, A. H. G. David, P. J. Das, D. J. Pe, J. F. Stoddart, *Chem. Soc. Rev.* **2022**, *51*, 5557–5605.
[7] X. N. Han, Y. Han, C. F. Chen, *Chem. Soc. Rev.* **2023**, *52*, 3265–3298.
[8] M. Mastalerz, *Acc. Chem. Res.* **2018**, *51*, 2411–2422.
[9] S. Ito, H. Takata, K. Ono, N. Iwasawa, *Angew. Chem. Int. Ed.* **2013**, *52*, 11045–11048.
[10] Y. Li, N. Li, G. Li, Y. Qiao, M. Zhang, L. Zhang, Q.-H. Guo, G. He, *J. Am. Chem. Soc.* **2023**, *145*, 9118–9128.
[11] J. Chen, W. Zhang, W. Yang, F. Xi, H. He, M. Liang, Q. Dong, J. Hou, M. Wang, G. Yu, J. Zhou, *Nat. Commun.* **2024**, *15*, 1260.
[12] Y. Wang, K. Xu, B. Li, L. Cui, J. Li, X. Jia, H. Zhao, J. Fang, C. Li, *Angew. Chem. Int. Ed.* **2019**, *131*, 10387–10390.
[13] J.-R. Wu, G. Wu, D. Li, D. Dai, Y.-W. Yang, *Sci. Adv.* **2022**, *8*, eabo2255.
[14] A. Dey, S. Chand, B. Maity, P. M. Bhatt, M. Ghosh, L. Cavallo, M. Eddaoudi, N. M. Khashab, *J. Am. Chem. Soc.* **2021**, *143*, 4090–4094.
[15] J. Wu, B. Li, Y. Yang, *Angew. Chem. Int. Ed.* **2020**, *132*, 2271–2275.
[16] D. Wang, Y. Zhao, *Angew. Chem. Int. Ed.* **2023**, *62*, e202217903.
[17] S. I. Kawano, M. Nakaya, M. Saitow, A. Ishiguro, T. Yanai, J. Onoe, K. Tanaka, *J. Am. Chem. Soc.* **2022**, *144*, 6749–6758.18.
[18] G. Pan, J. Liu, H. Zhang, L. Wan, Q. Zheng, C. Bai, *Angew. Chem. Int. Ed.* **2003**, *42*, 2747–2751.
[19] S. S. Jester, E. Sigmund, S. Höger, *J. Am. Chem. Soc.* **2011**, *133*, 11062–11065.
[20] T. Chen, G. B. Pan, H. Wettach, M. Fritzsche, S. Höger, L. J. Wan, H. B. Yang, B. H. Northrop, P. J. Stang, *J. Am. Chem. Soc.* **2010**, *132*, 1328–1333.
[21] J. D. Cojal González, M. Iyoda, J. P. Rabe, *Nat. Commun.* **2017**, *8*, 14717.
[22] J. C. Lauer, B. Kohl, F. Braun, F. Rominger, M. Mastalerz, *Eur. J. Org. Chem.* **2022**, e202101317.
[23] Y. S. Chan, H. Hayashi, S. Sato, S. Kasahara, K. Matsuo, N. Aratani, H. Yamada, *Eur. J. Org. Chem.* 2022, e202200621.
[24] S. Otto, R. L. E. Furlan, J. K. M. Sanders, *Science* **2002**, *297*, 590–593.
[25] P. T. Corbett, J. Leclaire, L. Vial, K. R. West, J. L. Wietor, J. K. M. Sanders, S. Otto, *Chem. Rev.* **2006**, *106*, 3652–3711.
[26] H. Hayashi, A. Sobczuk, A. Bolag, N. Sakai, S. Matile, *Chem. Sci.* **2014**, *5*, 4610–4614.
[27] R. J. Wojtecki, M. A. Meador, S. J. Rowan, *Nat. Mater.* **2011**, *10*, 14–27.
[28] A. Wilson, G. Gasparini, S. Matile, *Chem. Soc. Rev.* **2014**, *43*, 1948–1962.
[29] N. Christinat, R. Scopelliti, K. Severin, *Chem. Commun.* **2004**, *4*, 1158–1159.
[30] M. Lista, E. Orentas, J. Areephong, P. Charbonnaz, A. Wilson, Y. Zhao, A. Bolag, G. Sforazzini, R. Turdean, H. Hayashi, Y. Domoto, A. Sobczuk, N. Sakai, S. Matile, *Org. Biomol. Chem.* **2013**, *11*, 1754–1765.
[31] N. Christinat, R. Scopelliti, K. Severin, *Angew. Chem. Int. Ed.* **2008**, *47*, 1848–1852.
[32] Y. Jin, Q. Wang, P. Taynton, W. Zhang, *Acc. Chem. Res.* **2014**, *47*, 1575–1586.
[33] F. B. L. Cougnon, A. R. Stefankiewicz, S. Ulrich, *Chem. Sci.* **2023**, *15*, 879–895.
[34] S. Ito, K. Ono, N. Iwasawa, *J. Am. Chem. Soc.* **2012**, *134*, 13962–13965.
[35] N. Iwasawa, H. Takahagi, *J. Am. Chem. Soc.* **2007**, *129*, 7754–7755.
[36] G. Zhang, O. Presly, F. White, I. M. Oppel, M. Mastalerz, *Angew. Chem. Int. Ed.* **2014**, *53*, 1516–1520.
[37] S. Klotzbach, F. Beuerle, *Angew. Chem. Int. Ed.* **2015**, *54*, 10356–10360.
[38] M. Rondelli, S. Delgado-Hernández, A. H. Daranas, T. Martín, *Chem. Sci.* **2023**, *14*, 12953–12960.
[39] M. Rondelli, J. Pasán, I. Fernández, T. Martín, *Chem. Eur. J.* **2024**, *30*, e202400896.
[40] S. Klotzbach, T. Scherpf, F. Beuerle, *Chem. Commun.* **2014**, *50*, 12454–12457.
[41] N. Nishimura, K. Kobayashi, *Angew. Chem. Int. Ed.* **2008**, *47*, 6255–6258.
[42] A. P. Côté, A. I. Benin, N. W. Ockwig, M. O'Keeffe, A. J. Matzger, O. M. Yaghi, *Science* **2005**, *310*, 1166–1170.
[43] H. Hayashi, Y. Kato, A. Matsumoto, S. Shikita, N. Aizawa, M. Suzuki, N. Aratani, T. Yasuda, H. Yamada, *Chem. Eur. J.* **2019**, *25*, 15565–15571.
[44] J. Zhu, H. Hayashi, M. Chen, C. Xiao, K. Matsuo, N. Aratani, L. Zhang, H. Yamada, *Macromol. Chem. Phys.* **2021**, *222*, 2100024.
[45] M. Chen, L. Yan, Y. Zhao, I. Murtaza, H. Meng, W. Huang, *J. Mater. Chem. C* **2018**, *6*, 7416–7444.
[46] D. F. Chen, Y. Han, *Acc. Chem. Res.* **2018**, *51*, 2093–2106.
[47] C. B. Du, Y. J. Long, X. N. Han, Y. Han, C. F. Chen, *Chem. Commun.* **2024**, *60*, 13492–13506.
[48] T. Ogoshi, S. Takashima, T. A. Yamagishi, *J. Am. Chem. Soc.* **2015**, *137*, 10962–10964.
[49] H. Hayashi, J. Zhu, N. Minamino, Y. Murakami, S. Kasahara, K. Matsuo, N. Aratani, H. Yamada, *Eur. J. Org. Chem.* **2024**, e202400770.
[50] Crystallographic data for **Ant-Ph**: $C_{61}H_{73}O_4B_2Cl_3Si_2$, M_w = 1054.34, Orthorhombic, space group $Pca2_1$, a = 18.8994(3), b = 20.8600(4), C = 29.4360(5) Å, V = 11604.9(3) Å^3, T = 103 K, Z = 8, reflections measured 189521, 26574 unique. The final R_1 was 0.0600 ($I > 2\sigma(I)$), and the final wR on F^2 was 0.1494 (all data), GOF = 1.051.
[51] H. Takahagi, N. Iwasawa, *Chem. Eur. J.* **2010**, *16*, 13680–13688.
[52] S. Y. Ding, W. Wang, *Chem. Soc. Rev.* **2013**, *42*, 548–568.
[53] B. Shi, J. Jiang, H. An, L. Qi, T. B. Wei, W. J. Qu, Q. Lin, *J. Am. Chem. Soc.* **2024**, *146*, 2901–2906.
[54] H. Yao, Y. M. Wang, M. Quan, M. U. Farooq, L. P. Yang, W. Jiang, *Angew. Chem. Int. Ed.* **2020**, *59*, 19945–19950.
[55] J. Zhou, G. Yu, Q. Li, M. Wang, F. Huang, *J. Am. Chem. Soc.* **2020**, *142*, 2228–2232.
[56] K. Jie, Y. Zhou, E. Li, R. Zhao, M. Liu, F. Huang, *J. Am. Chem. Soc.* **2018**, *140*, 3190–3193.
[57] F. Zeng, L. Cheng, W. J. Zhang, L. L. Tang, X. F. Wang, *Org. Chem. Front.* **2022**, *9*, 3307–3311.
[58] D. W. Zhang, X. Zhao, J. L. Hou, Z. T. Li, *Chem. Rev.* **2012**, *112*, 5271–5316.
[59] Z. Liu, Y. Zhou, L. Yuan, *Org. Biomol. Chem.* **2022**, *20*, 9023–9051.
[60] S. Huang, X. Li, Y. Cai, W. Feng, L. Yuan, *Chem. Eur. J.* **2024**, *30*, e202303394.
[61] T. A. Sobiech, Y. Zhong, B. Gong, *Org. Biomol. Chem.* **2022**, *20*, 6962–6978.
[62] W. Zhang, J. S. Moore, *Angew. Chem. Int. Ed.* **2006**, *45*, 4416–4439.

Manuscript received: January 9, 2025
Revised manuscript received: February 25, 2025
Accepted manuscript online: March 2, 2025
Version of record online: April 4, 2025